Article:
Peretti, G. orcid.org/0009-0004-3913-5508, Bouscharain, N. and Dwyer-Joyce, R. orcid.org/0000-0001-8481-2708 (2025) In-situ ultrasonic viscometry of lubricants under high-pressure and high-shear. Rheologica Acta. ISSN: 0035-4511

https://doi.org/10.1007/s00397-025-01516-9

Rheologica Acta
https://doi.org/10.1007/s00397-025-01516-9

ORIGINAL CONTRIBUTION

In-situ ultrasonic viscometry of lubricants under high-pressure and high-shear

Gladys Peretti[1] · **Nathalie Bouscharain**[2] · **Robert Dwyer-Joyce**[1]

Received: 12 June 2025 / Revised: 15 July 2025 / Accepted: 20 July 2025

Abstract
Viscosity affects lubricant film thickness and the separation of machine parts. It is thus a major parameter to ensure adequate lubrication and machine operation. Viscosity is dependent on operating conditions, especially pressure, which is known to vary up to several GPa in tribological contacts. Few viscometers are capable of performing in-situ measurements, and replicating the combined extreme operating conditions outside the contact zone is difficult. This work employs ultrasound to enable in-situ viscosity measurements under high-pressure and high-shear. The low-shear viscosity behaviour under pressure of distilled water, octane, squalane (SQL), squalane + polyisoprene (SQL+PIP), diisodecylphthalate (DidP), and polyalphaolefin 100 (PAO100) was derived from the literature using the Williams-Landel-Ferry-Yasutomi (WLF-Yasutomi) model. Combined with shear-thinning models from the literature, the viscosity under high-pressure and high-shear ($4.5 \times 10^6\ s^{-1}$) was determined. An ultrasonic viscometer was instrumented onto a high-pressure test cell. Several fluids were used to calibrate the ultrasonic viscometer under pressure. The ultrasonic viscosities of SQL+PIP and PAO100 were computed at 40 °C, from ambient pressure up to 600 MPa, and compared with literature data. This work contributes to a better understanding of the ultrasonic in-situ viscometry technique. Such insight is crucial to apply this technique to challenging environments. The ultrasonic viscometer also holds significant potential to advance the understanding of complex fluids under high-pressure and high-shear conditions, where conventional measurement methods often fall short. Moreover, the ultrasonic viscometry technique has strong potential for industrial application, where there is a growing need for real-time, in-situ monitoring of fluid properties under varying operating conditions. This can lead to improved process control, safety, and efficiency across a range of industries.

Keywords Shear viscosity · High-pressure · Shear-thinning · Ultrasound · Lubricant

Introduction

In industrial applications such as bearings, lubricants form a very thin film between moving parts and prevent wear. In this elasto-hydrodynamic lubrication regime, pressures can reach several GPa (Vergne 2008). The behaviour of lubricants, especially their viscosity, under such pressures needs to be understood.

✉ Gladys Peretti
gperetti1@sheffield.ac.uk

[1] The Leonardo Centre for Tribology, The University of Sheffield, Sheffield, UK

[2] INSA Lyon, CNRS, LaMCoS, UMR5259, Villeurbanne 69621, France

However, few conventional viscometers can operate under pressures higher than 50 MPa. Those that can, such as falling-body viscometers, are labour-intensive, require strict operating and cleaning protocols, and often involve lengthy test durations. Additionally, they are not suited for online measurements, particularly not in the tribological contact. Ultrasound presents a complementary in-situ approach with relatively simple equipment. This work aims to demonstrate the feasibility of using ultrasound to perform viscosity measurements under high-pressure and high-shear, addressing key limitations of conventional methods.

First, the equipment used to pressurise fluids and acquire data are presented. Then, the experimental method is detailed, and the ultrasonic viscosity results under high-pressure and high-shear are laid out. Finally, the literature models used

Published online: 10 September 2025

to describe the viscosity behaviour under high-pressure and high-shear are described in the appendix.

Ultrasound, apparatus and fluids

Ultrasound viscometry

The ultrasonic viscosity measurement technique is based on reflectrometry, which is the reflection and transmission of acoustic waves at the interface between two media. The technique has been used in previous work to measure fluid viscosity (Peretti et al. 2023; Schirru et al. 2015). A shear ultrasonic transducer is bonded onto a metal part, itself in contact with the fluid sample, forming a 2-layer system. A shear ultrasonic wave is emitted by the transducer; it travels through the metal part. At the interface between the metal and the fluid, it is both transmitted and reflected. The reflected wave is measured by the same transducer (pulse-echo setup). The reflection coefficient R describes the amount of reflected energy. It is defined as $R = \frac{z_2 - z_1}{z_2 + z_1}$, with z_1 and z_2 the acoustic impedances of both media. When the media are a solid and a liquid, there is an acoustic impedance mismatch leading to $R \approx 1$. The reflected wave is very similar to the emitted one: the measurement is not sensitive to the fluid properties, especially its viscosity.

To tackle this problem, an intermediate layer called matching layer was added by Schirru et al. (2015) to create a 3-layer system. The matching layer is a thin film of polymer; its role is to increase the amount of energy transmitted to the lubricant. The reflection coefficient R is theoretically described with Eq. 1, with z_i the acoustic impedances of each medium, k_2 the wavenumber of the matching layer, and L_2 the thickness of the matching layer. Experimentally, the reflection coefficient is computed by dividing the frequency-domain signal from the sample of interest by the one of the reference (2).

$$R = \frac{(z_2 z_3 - z_1 z_2)\cos(k_2 L_2) + i(z_2^2 - z_1 z_3)\sin(k_2 L_2)}{(z_2 z_3 + z_1 z_2)\cos(k_2 L_2) + i(z_2^2 + z_1 z_3)\sin(k_2 L_2)} \tag{1}$$

$$R = \left.\frac{\text{signal sample}}{\text{signal reference}}\right|_{\text{frequency-domain}} \tag{2}$$

The reflection coefficient R can be linked to the viscosity η through a calibration: $R = x_0 \times ln(\eta) + x_1$, with x_0 and x_1 constants. The reflection coefficient of unknown fluids can then be measured and their viscosity calculated.

High-pressure cell

The test fluids were pressurised in a **high-pressure cell**, which is a complex assembly of several parts (Fig. 1) based on the work of Bair (2000). The pressure cell was located at AC2T in Austria. The main part is the high-pressure vessel–a steel chamber with thick walls that was designed to withstand pressures up to 1.3 GPa. A membrane made of nitrile rubber separates the test fluid from the pressurising fluid.

A **piston** separates the fluids from pump 1 and from pump 2 using three stacked seals made of different materials: rubber, plastic, and metal. The rubber seal is softer and is efficient at lower pressures. When the pressure gets higher, the plastic seal becomes active and prevents leaks. As the pressure keeps increasing, the metal seal is the one ensuring there are no leaks. The piston serves as a pressure amplifier. The piston position is determined by a force equilibrium on both sides: $F_1 = F_2$, which means $p_1 A_1 = p_2 A_2$, with F the forces, p the pressures, A the areas, and the indices 1 and 2 referring to the pressurising fluid on both sides of the piston. The rig was designed with a 50:1 ratio, so $A_2 = 50 A_1$, which means

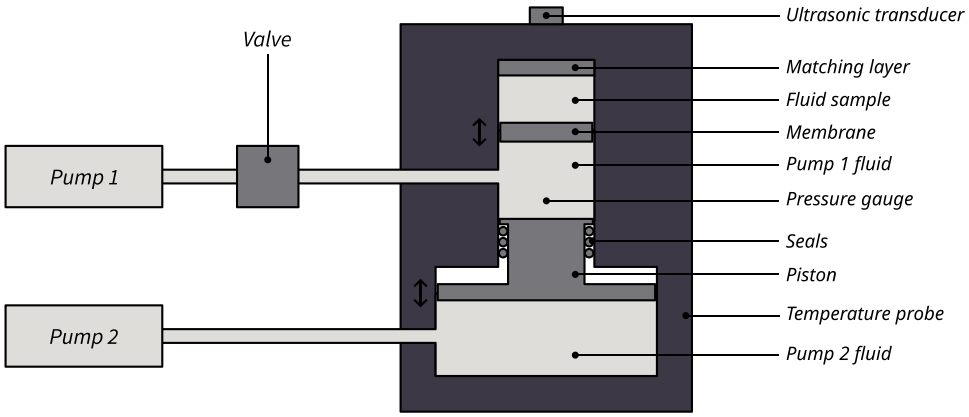

Fig. 1 The high-pressure cell instrumented with ultrasonic equipment

that $p_1 = 50 p_2$. For a given pressure p_2, the resulting pressure p_1 is 50 times higher. A heating collar sets and controls the chamber temperature. Two Enerpac P39 pumps, that can each reach a 70 MPa pressure, are connected to the pressure chamber. A valve protects pump 1 from the pressure in the chamber.

Several devices are used to **record** the data. A high-pressure gauge (P3MB BlueLine from HBK) measures and records the pressure up to 1.5 GPa through a pressure DAq (NI-9237). A temperature probe records the temperature. Due to the sealed, pressurised environment, the temperature probe is not directly in contact with the lubricant. Instead, the probe measures the temperature of the high-pressure chamber wall. As the chamber is a voluminous steel block, a heating latency is taken into account for the sample and no testing is performed before temperature equilibrium is reached. Additionally, a 8 MHz shear ultrasonic transducer is bonded on the outside of the high-pressure chamber. Facing the transducer and in contact with the test fluid, a 50 µm matching layer is bonded.

Test fluids

To assess the feasibility of ultrasonic viscosity measurement under pressure, it was essential to use test fluids with well-characterised viscosity behaviour under pressure. Moreover, fluids that were easy and safe to manipulate, and that covered a wide viscosity range were preferred to facilitate future deployment. The chosen fluids were distilled water, octane, squalane (SQL), squalane + polyisoprene (SQL+PIP), diisodecylphthalate (DidP), and polyalphaolefin 100 (PAO100).

The **low-shear viscosity** was described for all fluids in the operating condition ranges of interest using the Vogel-Fulcher-Tammann (VTF) and the Williams-Landel-Ferry-Yasutomi (WLF-Yasutomi) models. Distilled water is a low-viscosity fluid and its viscosity scarcely increases with pressure. Octane, SQL, SQL+PIP, DidP, and PAO100 display a common behaviour with a decreasing viscosity gradient between ambient pressure and 200 MPa (concave curve), followed by a constant logarithm viscosity gradient (straight line).

However, ultrasound waves are shear waves. According to the Cox-Merz law, the shear rate can be equivalent to the ultrasonic frequency, i.e. $4.5 \times 10^6\,\mathrm{s}^{-1}$ (Cox and Merz 1958). At this shear rate, some fluids exhibit a non-Newtonian behaviour. The **high-shear viscosity** was estimated by applying shear-thinning models to the WLF-Yasutomi viscosity data. This approach was chosen for practical reasons; however, it should not be used to extrapolate high-shear viscosities beyond the current temperature and pressure range. Water and octane were considered to be Newtonian fluids, and no shear-thinning information was found in the literature about DidP. For the other test fluids, the high-shear viscosities are equal or lower than their low-shear counterparts.

Detailed information about the models is available in Appendix A, and the viscosity-pressure behaviour at 40 °C is shown in Fig. 2. The viscosities of the studied fluids span 7 decades across the pressure range.

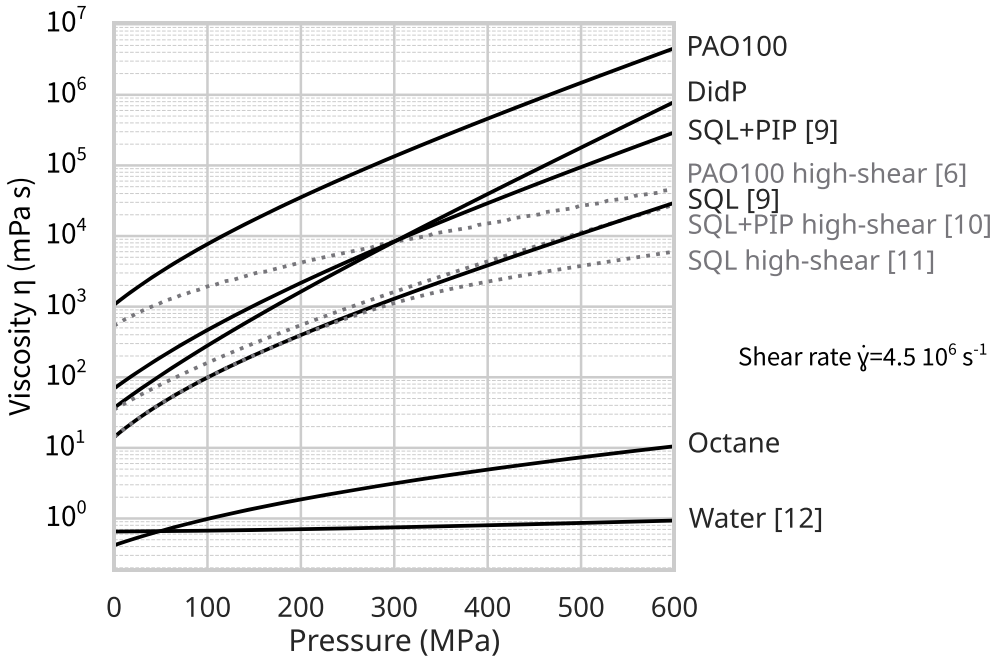

Fig. 2 Viscosity-pressure behaviour at low and high shear for the test fluids at 40 °C

None of the fluids are controlled commercially-available calibration fluids: their viscosity varies for each batch. Both SQL and SQL+PIP were proposed as reference fluids by Bair (2006). SQL is a low-viscosity base oil; the sample used in the present work had a purity of 99%. The additive PIP is a viscosity modifier; the sample in this work was made from synthetic rubber and had a molecular weight of $\approx 40\,000\,\mathrm{g\,mol^{-1}}$. SQL+PIP was made using 85% SQL and 15% PIP in weight.

The **calibration** under pressure was performed using distilled water, octane, SQL, and DidP. The ultrasonic viscosities of SQL+PIP and PAO100 were measured and compared with the literature. SQL+PIP served as a **validation** fluid, while PAO100 was used to **explore** the limits of the ultrasonic viscometer.

Experimental method

High-pressure cell methodology

Before each test, the sample chamber was cleaned with ethanol and heptane. Approximately 5 mL of sample was then inserted in the sample chamber. The lid of the sample chamber was partially closed; the fluid was slowly pressurised and overflowed to prevent trapping air bubbles between the fluid and the matching layer.

The pressure cell was then brought to the desired temperature: 40 °C in the present application. A couple of hours were necessary for the whole cell and the lubricant to stabilise at the target temperature. Thermal capacity represents the amount of energy needed to increase the temperature of a liquid or solid by 1 °C. The thermal capacity of steel is $\approx 0.5\,\mathrm{kJ\,kg^{-1}\,K^{-1}}$ (The Engineering Toolbox 2003a) while that of lubricating oil is $\approx 2.1\,\mathrm{kJ\,kg^{-1}\,K^{-1}}$ (The Engineering Toolbox 2003b). At equivalent masses, lubricants require more energy than steel to get heated. The mass of the steel chamber is however significantly larger than the mass of the lubricants. Assuming that the steel chamber is 10 kg (low assumption) and that the lubricants weight 1 kg (high assumption), the energy needed to increase the temperature by 1 °C would be 5 kJ for steel and 2.1 kJ for lubricants. As it takes less energy to heat up the lubricants than the steel chamber, the temperature regulation and measurement approach was considered valid.

The valve was opened, and the piston was lowered using pump 1. The ultrasonic, pressure, and temperature acquisitions were started. Pump 1 was used for pressures up to 60 MPa, then the valve was closed to maintain this initial pressure. The second pump was then used to amplify the existing pressure up to 600 MPa.

The data was acquired at several pressure steps: ambient pressure, 50, 100, 150, 200, 300, 400, 500, and 600 MPa. Each pressure step was maintained for around 10 minutes to evaluate dynamic pressure effects. Once 600 MPa had been reached, the pressure was released, and the sample chamber was emptied. The whole process could be repeated with another sample.

Ultrasonic methodology

A 4.5 MHz sine wave of 4V peak-to-peak amplitude with 5 cycles was generated at each pressure step by the shear ultrasonic transducer every 10 seconds.

The **data processing** allowed the extraction of the reflection coefficient from each signal; it is presented in Fig. 3 for SQL. The raw time-domain signal, called AScan (subfigure a), is cropped to only keep the first reflection (subfigure b). The signal from the reference is in red, and the signals from the sample are in shades of blue: light blue for low pressures, and dark blue for high pressures. This first reflection is converted to a frequency-domain signal (subfigure c). The amplitude of the signal decreases as the pressure increases. Finally, the reflection coefficient is computed by dividing the signal from the fluid by the signal of the reference (subfigure d). The reflection coefficient is closer to 1 at low pressures, and closer to 0 at high pressures. Because the experiment was performed under pressure, several questions arose about the data processing and are studied in this work.

1. Dynamic pressure effects are considered in Section "Reflection coefficient results" to assess the accuracy of **averaging data over time**.
2. A **calibration** was performed using an air reference in Section "Calibration".

Temperature and pressure stability

As viscosity depends both on temperature and pressure, it was of utmost importance to reduce the variations of both parameters through the test duration.

The **temperature** was controlled by a heating collar. A small temperature variation leads to a significant change in viscosity, especially at low temperatures (40 °C and lower). A constant temperature is therefore of paramount importance. The quality of the regulation was verified during post-processing: the temperature evolution over time for SQL for each pressure step is plotted in Fig. 4. The temperatures all lie around 40 °C, which highlights a good precision and shows that pressure does not have an impact on temperature. Each temperature curve is cyclic, with a maximum amplitude of 0.15 °C, emphasising a good accuracy. The same temperature behaviour was found for all fluids, and the control was considered stable enough for this application.

The **pressure** was manually set by an operator during the tests and was kept constant for each step. The pressure

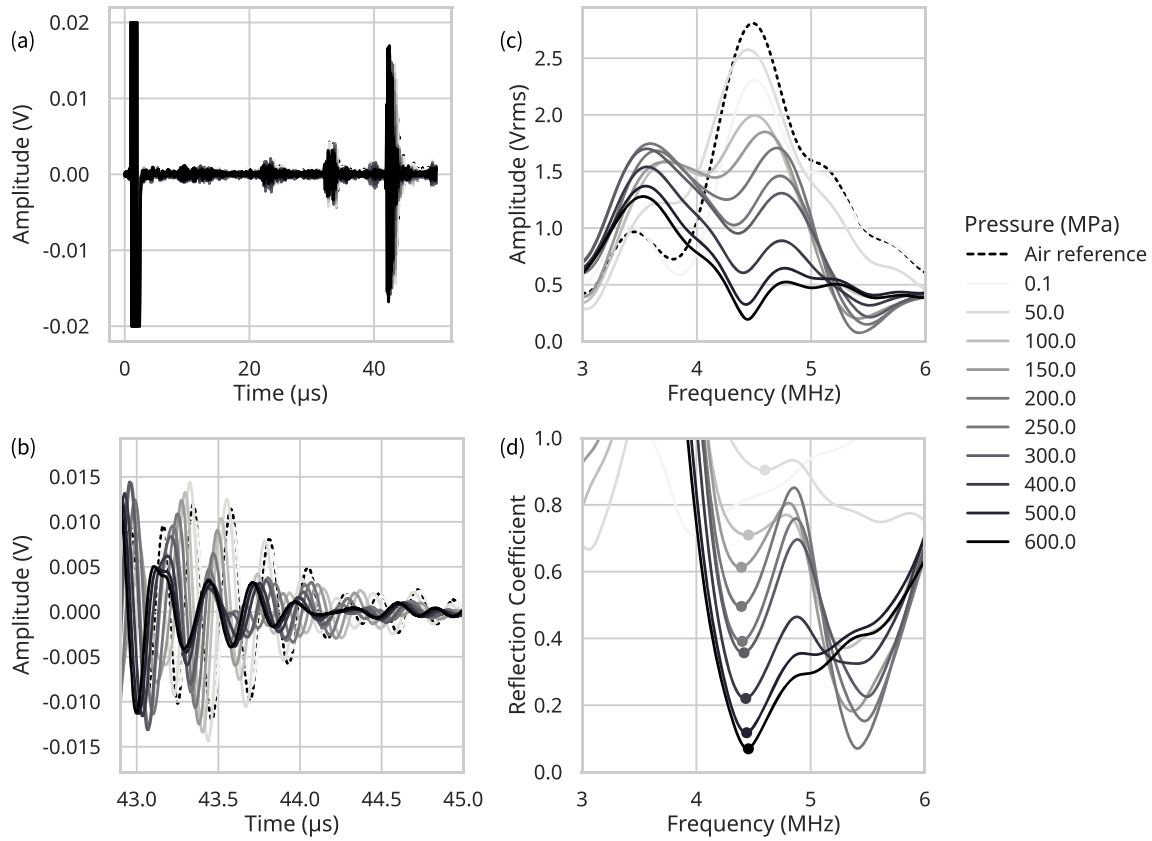

Fig. 3 Ultrasonic data processing for SQL: (a) AScan, (b) cropped AScan, (c) frequency-domain signal, (d) reflection coefficient

measurements are shown in Fig. 4 for SQL. Leakage was non-existent for most pressure steps, but between 100 MPa and 300 MPa. These leaks were probably due to the multi-seal design of the piston: the intermediate plastic seal was not perfectly preventing leakage in the mid-pressure range. Two methods were used to mitigate the impact of leakages: 1. manual pressure adjustments during testing, 2. data removal during post-processing when the measured pressure was off by more than ± 20 MPa.

Viscosity-pressure results

Reflection coefficient results

In the present section, the reflection coefficient is calculated using (2) with air as the reference fluid. In Fig. 3d, the reflection coefficient decreases as the pressure increases, while its frequency does not seem to follow a trend. However, since Fig. 3 displays only a single signal per pressure step, these observations require further validation.

Firstly, the impact of **dynamic pressure effects** needs to be ruled out. To do so, the reflection coefficient of SQL for each pressure step is plotted as a function of time in Fig. 5a. For each pressure step, the reflection coefficient remains mostly constant over time. The variations can be directly linked to pressure changes due to leakage (see Fig. 4b). This means that there are no dynamic pressure effects. The reflection coefficient can thus be averaged over time for each pressure step.

Then, in Fig. 5b, the averaged reflection coefficient is presented as a function of the **resonance frequency**. The error bars inform of the maximum and minimum values at each pressure step for both axes. The resonance frequency is mostly constant across the pressure steps, but for the ambient pressure data.

Method limits

Both plots of Fig. 5 demonstrate the sensibility of ultrasonic measurement under pressure, however, there appear to be some limitations.

The behaviour at **ambient pressure** does not fit the rest of the data. First, the reflection coefficient at ambient pressure is lower than the one at 50 MPa. Second, the resonance frequency at ambient pressure is misaligned with the other pressure steps. A possible explanation for this behaviour comes from the test apparatus. As seen in Fig. 1, the matching layer is positioned above the sample. This is not an issue when testing under pressure, as the lubricant is pushed against the

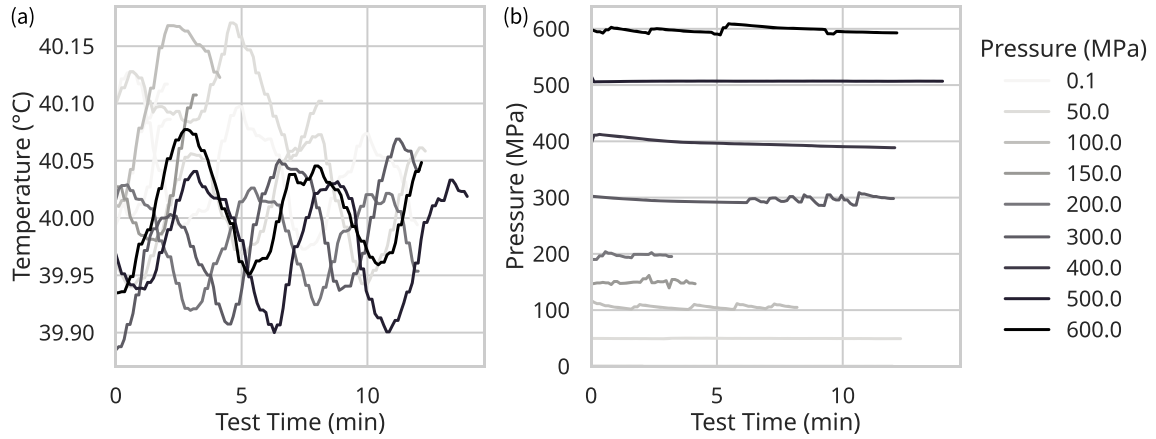

Fig. 4 Operating conditions over time for SQL: (a) temperature, (b) pressure

matching layer. However, at ambient pressure, there might be no or imperfect contact between the fluid and the matching layer due to the presence of air bubbles, resulting in non-accurate measurements. The ambient pressure data is not shown in the rest of this paper. It is recommended to improve the experimental protocol and turn the test cell upside-down during future testing.

Another limit of the measurement is the **maximum pressure or viscosity** that the setup is sensitive to. The reflection coefficient for SQL between 50 MPa and 600 MPa decreases from 0.90 to 0.06. The behaviour of the reflection coefficient as it approaches 0 is discussed later on.

Calibration

Air reference: calibration per pressure steps

The first set of fluids that was tested are calibration fluids: their low-shear viscosity behaviour under pressure is known from the literature. When available, the high-shear data is used. The measured reflection coefficients can thus be linked with the known viscosities to calibrate the apparatus. The low-shear data for distilled water and the steady high-shear data for SQL are presented in Fig. 6. For both fluids, reflection coefficient decreases as viscosity increases. For water, although its viscosity does not vary much with pressure (from 0.65 mPa s at ambient pressure to 0.93 mPa s at 600 MPa), its reflection coefficient varies from 0.90 to 0.25.

At a given viscosity but under different pressures, the reflection coefficient R varies. This suggests that beyond viscosity, the reflection coefficient is sensitive to the nature of the fluid and pressure-related effects such as the compression of the matching layer.

The test cell is thus **calibrated** using distilled water, octane, SQL, and DidP. The data for DidP is used up to 300 MPa as it displays a reflection coefficient inversion at higher pressures. Logarithmic calibration curves are fitted to the data for each pressure step: $R = x_0 \times ln(\eta) + x_1$ with R the reflection coefficient, η the dynamic viscosity, and $x_0(p)$ and $x_1(p)$ pressure-dependent constants (Fig. 7). The curves are

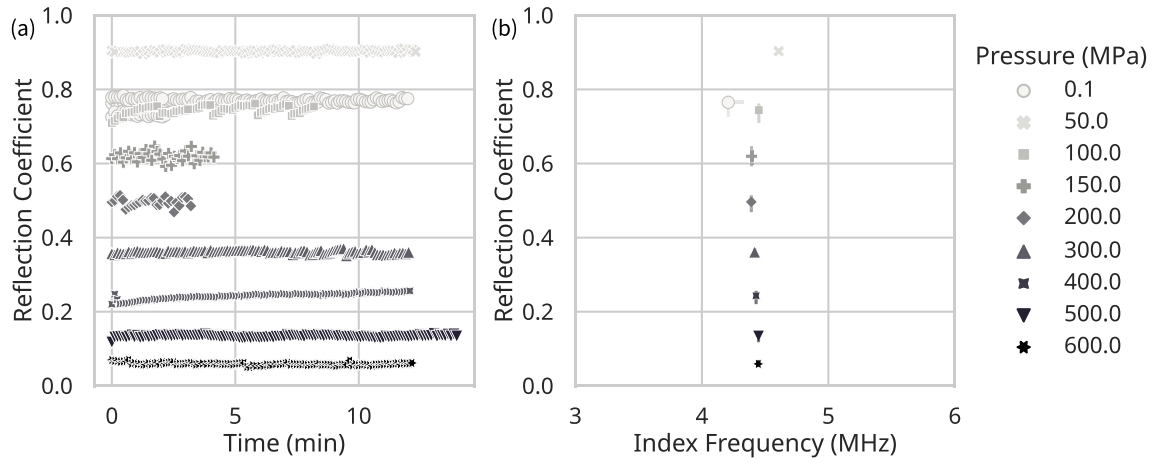

Fig. 5 Reflection coefficient of SQL: (a) as a function of time, (b) versus resonance frequency

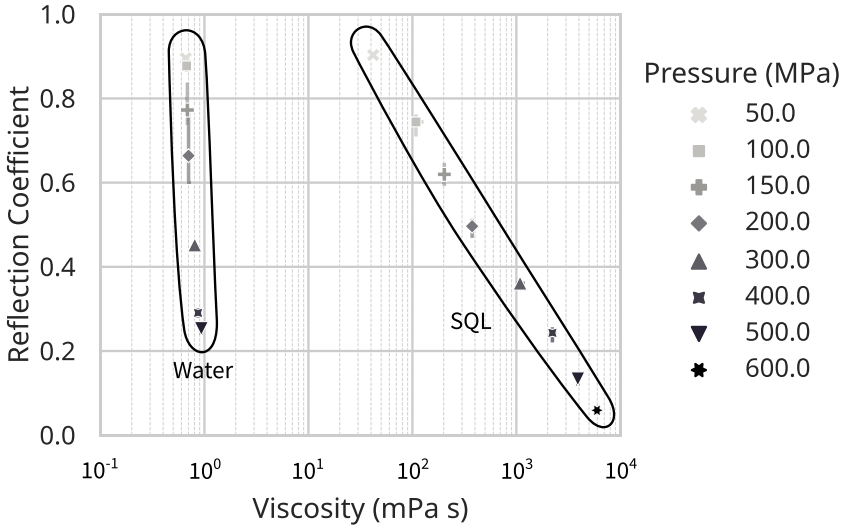

Fig. 6 Measured reflection coefficient versus viscosity from literature for distilled water and SQL. The steady shear viscosity of SQL (Bair et al. 2014) is used at $\dot{\gamma} = 4.5 \times 10^6\ \mathrm{s}^{-1}$

nearly parallel to one another, with the lowest pressure at the top and the highest pressure at the bottom.

The fit quality is assessed using the Pearson correlation coefficient r computed between the reflection coefficient R and $\ln(\eta)$ (*corr* function in Python Pandas). The correlation coefficient r evaluates how well the transformed data follows a linear relationship. The **determination coefficient** r^2 evaluates the proportion of variance explained by the fit (Table 1). The determination coefficients are mostly > 0.85, which highlights good fits. However, the fit quality is limited by the small number of calibration fluids (only 4) despite a wide viscosity range spanning over 4 decades.

Validation with SQL+PIP

The **reflection coefficient** of SQL+PIP under pressure is measured using ultrasound and displayed in Fig. 8a. As anticipated, the reflection coefficient decreases with increasing viscosity.

The **ultrasonic viscosity** is then computed using the per-pressure calibration. In Fig. 8b, the ultrasonic viscosity is plotted with green markers, the low-shear literature viscosity from Bair et al. (2018) is plotted with a solid line, while the steady high-shear viscosity (Bair 2006) at $4.5 \times 10^6\ \mathrm{s}^{-1}$ is a dotted line (see Appendix A). The ultrasonic viscosity increases with increasing pressure, and shows good agreement with the high-shear literature viscosity. The ultrasonic data point at 150 MPa stands out from the trend. It is due to the calibration curve at 150 MPa having a greater negative slope than the others. Improving the calibration at this pressure would resolve the issue. The overall result for SQL+PIP validates the use of the ultrasonic viscometer under pressure.

The ultrasonic viscometer is capable of measuring the viscosity under pressure. Some key considerations when

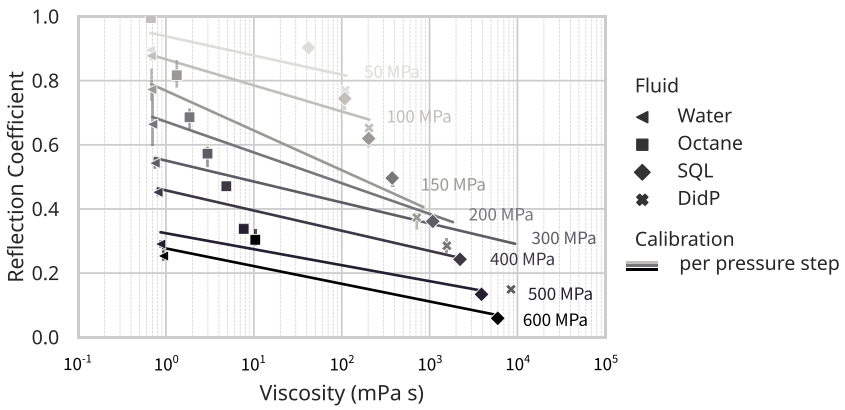

Fig. 7 Air-referenced calibration for each pressure step. The steady high-shear viscosity of SQL was used

Table 1 Determination coefficient between the reflection coefficient R and $\ln(\eta)$ for each pressure step

Pressure (MPa)	Determination Coefficient r^2
50	0.574
100	0.918
150	0.898
200	0.852
300	0.896
400	0.975
500	0.824
600	0.767

measuring the ultrasonic viscosity of other samples are proposed:

- The steady shear from the literature is difficult to compare with the ultrasonic shear. Moreover, there is no certainty that the Cox-Merz rule applies at such high frequencies and that the effective ultrasonic shear rate is $4.5 \times 10^6\ \mathrm{s}^{-1}$.
- The calibration is not perfect; using additional calibration fluids is necessary to increase the ultrasonic viscosity measurement accuracy.
- There is an uncertainty on the behaviour of the reflection coefficient near 0. This behaviour is studied in the following section with a fluid of higher viscosity.

Reflection coefficient inversion with PAO100

The **reflection coefficient** of PAO100 is studied in Fig. 9a: it initially decreases with increasing pressure, followed by an unexpected reversal. This reflection coefficient inversion has not been previously observed and its impact on viscosity measurements remains uncertain. One possibility would be to enhance the post-processing method to extract viscosity information despite the inversion. For example, by analysing the phase of the reflection coefficient. Otherwise, if the inversion prevents the viscosity measurement, the instrumentation could be modified to eliminate the phenomenon. Pulsing an ultrasonic transducer of a different frequency, and adjusting the thickness and material of the matching layer, would shift the reflection coefficient. These parameters should be optimised based on the expected viscosity range of the test fluids.

The **ultrasonic viscosity** of PAO100 was computed using the per-pressure calibration and is plotted as a function of pressure in Fig. 9b. The ultrasonic viscosity behaviour of PAO100 deviates significantly from trends predicted by the literature models. This discrepancy arises because the calibration curves were established using fluids with reflection coefficients and viscosities that fall well outside the range exhibited by PAO100. As a result, small inaccuracies in the slope of the calibration curve can lead to large errors when measuring highly viscous fluids like PAO100. For example, at 150 MPa, the calibration curve is based on a maximum viscosity of $\approx 10^2$ mPa s, corresponding to a reflection coefficient of 0.8, whereas PAO100 exhibits a reflection coefficient of 0.5 at the same pressure. This mismatch accounts for the poor accuracy in the viscosity of PAO100 and highlights the need to procure additional calibration fluids, particularly viscous ones.

Conclusion

The objective of this work was to perform ultrasonic viscosity measurement under pressure. The testing was performed at 40 °C from ambient pressure up to 600 MPa. The ultrasonic shear rate was estimated to be $4.5 \times 10^6\ \mathrm{s}^{-1}$ based on the Cox-Merz law. The temperature and pressure con-

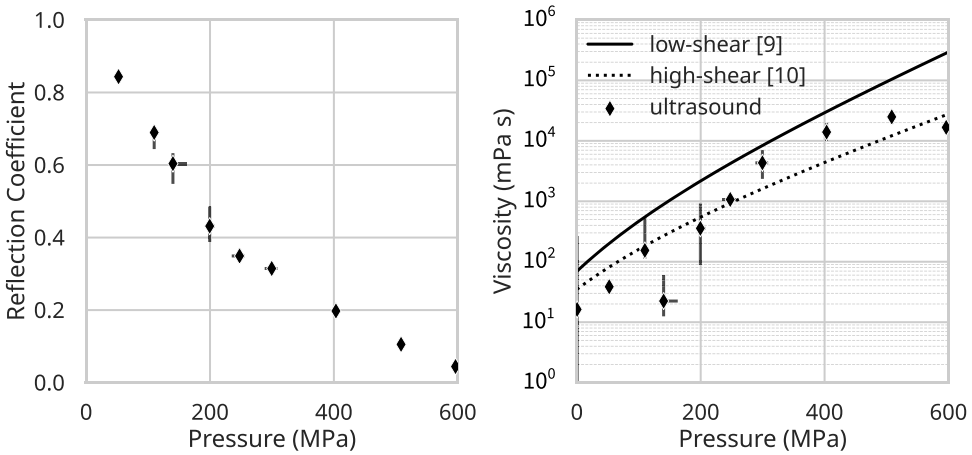

Fig. 8 Ultrasonic measurements of SQL+PIP under pressure: (a) reflection coefficient, (b) ultrasonic viscosity compared to low and high-shear models from the literature

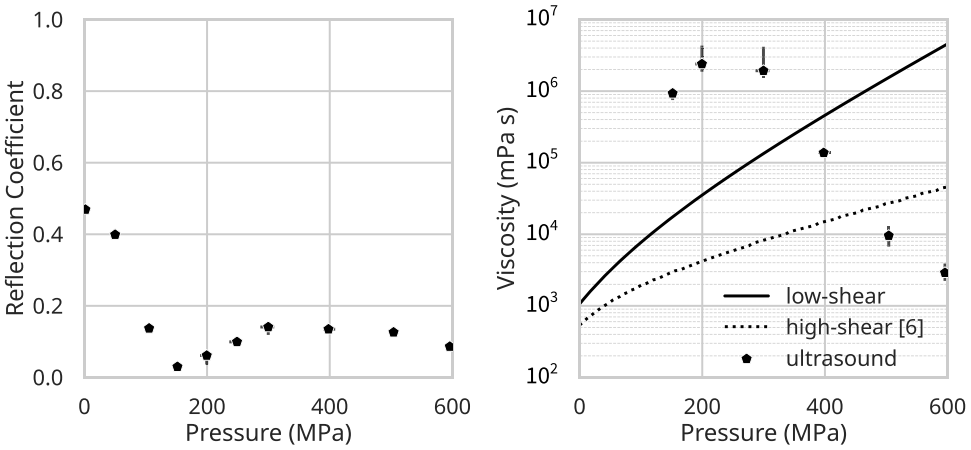

Fig. 9 Ultrasonic measurements of PAO100 under pressure: (a) reflection coefficient, (b) ultrasonic viscosity compared to low and high-shear models from the literature

ditions were monitored and deemed good enough for the current application. Fluids of known viscosity behaviour under high-pressure and high-shear were used to calibrate the viscometer. Ultrasonic viscosity measurements were performed for 2 fluids and compared with literature data.

The following results were drawn from the experiment:

- **Reflection coefficient**. There is a clear impact of pressure on the measured ultrasonic signal: the amplitude of the reflection coefficient decreases as the pressure increases. There are no dynamic pressure effects, which opens the possibility to perform dynamic measurements under varying pressures.
- **Calibration and reference**. An air-referenced calibration was performed and was found to be dependent on fluid properties beyond viscosity. One calibration per pressure step was thus required.
- **Viscosity**. The viscosity of SQL+PIP was measured up to 600 MPa and was in agreement with the high-shear viscosity from the literature. It validates the use of the ultrasonic viscometer under pressure.
- **Reflection Coefficient Inversion**. The ultrasonic viscosity of PAO100, a viscous fluid, was measured up to 600 MPa. It featured a reflection coefficient inversion and highlighted the need for additional calibration fluids.

Further work is required to build on these results:

- Improve the cell design to expand the pressure range available for testing. Instrument more frequencies/matching layers to increase the range of measurable viscosities.
- Modify the ambient pressure testing. It is proposed that the cell is turned upside down during tests to prevent any air bubbles to be trapped between the fluid and the matching layer.
- Identify additional calibration fluids with well-defined viscosity behaviour under high-pressure and high-shear conditions.
- Understand how the ultrasonic shear impacts the viscosity measurements of shear-thinning fluids.

To conclude, the ultrasonic viscometer is capable of measuring viscosity under pressure. Compared to conventional methods for measuring viscosity under pressure, ultrasonic viscometry could perform in-situ measurements. This would allow real-time measurements under real tribological conditions, such as in monitoring applications.

Appendix A: Low and high-shear viscosity behaviour under pressure

This appendix details how the low and high shear viscosity behaviour under pressure of the test fluids was obtained from experimental data available in the literature. First, the literature data was gathered. Second, the low-shear viscosity under pressure was determined using the Vogel-Fulcher-Tammann (VTF) equation and the Williams-Landel-Ferry-Yasutomi (WLF-Yasutomi) model. Finally, the high-shear viscosity was determined using the Carreau model when available. This provided the viscosity data to calibrate the ultrasonic viscometer.

A.1 Literature viscosity data

The test fluids were distilled water, octane, squalane (SQL), squalane+polyisoprene (SQL+PIP), diisodecylphthalate (DidP), and polyalphaolefin 100 (PAO100). These fluids

were selected because they have been extensively studied in the literature. They are however not calibration fluids. This means that their viscosity is not standard and can vary from one batch to another.

Viscosity data first needed to be gathered for each fluid over wide temperature and pressure ranges. Depending on the fluid, different methods were used to obtain the V-T-p behaviour. The WLF-Yasutomi model (Bair et al. 2013) is described in this appendix for octane, DidP, PAO100, as well as SQL and SQL+PIP. Some data choices were made to improve the fits.

The data for **octane** came from Caudwell et al. (2009), Dymond and Young (1981), Oliveira and Wakeham (1992), Harris et al. (1997), Doolittle and Peterson (1951), Giller and Drickamer (1949), Madge (1930), Thorpe and Rodger (1894). Octane evaporates quickly, and is thus difficult to work with at higher temperatures. For this reason, the data above 100 °C was discarded.

The WLF models for **SQL** and **SQL+PIP** were readily available from Bair et al. (2018). The models are verified with the data from Bair (2006, 2002), Bair et al. (2018), Schmidt et al. (2015), Irving and Barlow (1971), Krahn and Luft (1994), Pensado et al. (2006), Harris (2009), Ciotta et al. (2009), Comuñas et al. (2013), Comuñas et al. (2014) for SQL, and Bair (2006) for SQL+PIP.

The data for **DidP** was provided by Paredes et al. (2009), Harris and Bair (2007), Motari et al. (2007), Caetano et al. (2004), Caetano et al. (2005), Fröba and Leipertz (2007). DidP is especially sensitive to changes in viscosity due to formulation difference in batches. In Harris and Bair (2007), only the data from sample B was used as it was the closest in formulation. Moreover, the data above 600 MPa was discarded as it was not used in the present application.

The viscosity of **PAO100** is derived from Nakamura et al. (2016), Liu et al. (2008), Bair and Flores-Torres (2019), Watts and Willette (1982). All the data was used for the VTF model, as it provided more points at ambient pressure. Only Liu et al. (2008) and Bair and Flores-Torres (2019) were used for the WLF model to focus on the pressure behaviour.

The data for **distilled water** was extracted from Huber et al. (2009). Only the data at 40 °C was used as it was the temperature of interest for the current application. An interpolation was applied and is detailed in this appendix.

A.2 Low-shear viscosity

A.2.1 VTF Equation

The Vogel-Fulcher-Tammann (VTF) equation links temperature T and viscosity η with A, B, and C fluid-specific constants (3). The constants A, B, and C can be determined if the viscosity is known for at least three distinct temperatures.

$$\eta = A \exp\left(\frac{B}{T - C}\right) \tag{3}$$

The glass transition describes a change in the physical properties of a solid material composed of polymers. The glass-transition temperature T_{g0} is the temperature at which this change happens. It was determined for each fluid by setting the viscosity at $\eta_g = 10^{12}$ Pas by convention and using the previously determined A, B, and C constants (4). The glass-transition temperature is needed in the WLF-Yasutomi model.

$$T_{g0} = \frac{B}{\ln\left(\frac{\eta_g}{A}\right)} + C \tag{4}$$

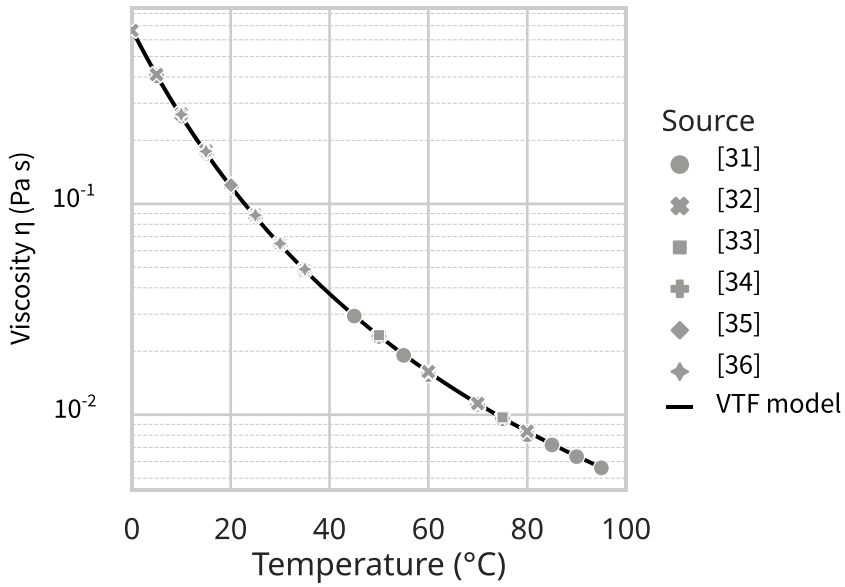

Fig. 10 Viscosity-temperature behaviour of DidP at ambient pressure

Table 2 VTF parameters

Parameter	unit	Octane	SQL (Bair et al. 2018)	SQL+PIP (Bair et al. 2018)	DidP	PAO100
A	Pa s	$4.40\,10^{-5}$	–	–	$7.102\,10^{-5}$	$6.72\,10^{-5}$
B	°C	490.90	–	–	795.031	1639.55
C	°C	−179.93	–	–	−86.844	−129.50
η_g	Pa s	10^{12}	$1.23\,10^{7}$	10^{12}	10^{12}	10^{12}
T_{g0}	°C	−166.90	−88.69	−73.62	−65.463	−85.47

In Fig. 10, the literature viscosity of DidP as a function of temperature was plotted with coloured markers. The black curve is the temperature-viscosity modelled behaviour of DidP at ambient pressure.

The parameters used for the VTF model for each fluid are summarised in Table 2.

A.2.2 WLF-Yasutomi Model

The viscosity-temperature-pressure behaviour for each fluid is then determined using the Williams-Landel-Ferry-Yasutomi (WLF-Yasutomi) model (5) (Bair et al. 2013). In this equation, η_g is the glass-transition viscosity, C_1 and C_2 are constants, and T is the temperature. Additionally, $T_g(p)$ and $F(p)$ are determined by Eqs. 6 and 7, respectively, where T_{g0} is the glass-transition temperature (determined with the VTF equation), p the pressure, and A_1, A_2, B_1, and B_2 are constants. The model is valid between T_{g0} and $T_{g0} + 300\,°C$ according to Yasutomi et al. (1984).

$$\eta(T,\,p) = \eta_g \exp\left(\log(10)\frac{-C_1\left(T - T_g(p)\right)F(p)}{C_2 + \left(T - T_g(p)\right)F(p)}\right) \quad (5)$$

$$T_g(p) = T_{g0} + A_1 \log(1 + A_2 p) \quad (6)$$

$$F(p) = (1 + B_1 p)^{B_2} \quad (7)$$

In Fig. 11, the literature viscosity of DidP as a function of temperature and pressure was plotted with coloured markers. The curves are the pressure-viscosity behaviour of DidP at a set temperature. The black curve is the pressure-viscosity at 40 °C, which is of interest in this application.

The viscosity-temperature-pressure behaviour can thus be determined over a temperature and pressure range. The parameters used for the WLF-Yasutomi model for each fluid are given in Table 3.

A.2.3 Interpolation

Water has a behaviour different to most oils under pressure: its viscosity range is small under pressure, and it has a convex shape under 400 MPa. For this reason, the WLF-Yasutomi model was not used. Instead, the interpolation function from Scipy in Python was used to interpolate data from the literature. Only the data at 40 °C was kept as it was the temperature of interest in this application. The results are shown in Fig. 12.

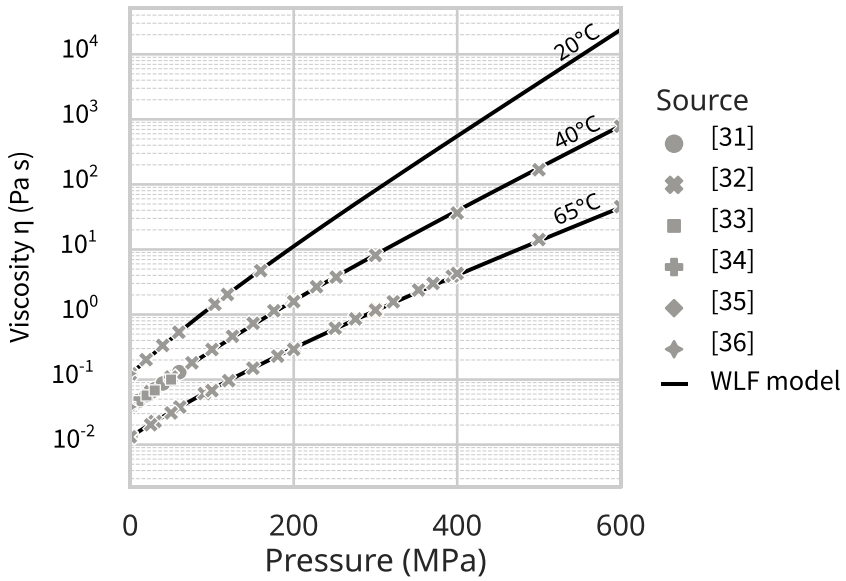

Fig. 11 Viscosity-temperature-pressure behaviour of DidP

Table 3 WLF-Yasutomi parameters

Parameter	unit	Octane	SQL (Bair et al. 2018)	SQL+PIP (Bair et al. 2018)	DidP	PAO100
A_1	°C	37.32	263.8	554.1	166.63	142.69
A_2	MPa^{-1}	0	$3.53\,10^{-4}$	$9.33\,10^{-5}$	$4.57\,10^{-4}$	$6.13\,10^{-4}$
B_1	MPa^{-1}	$1.130\,10^{-2}$	$1.37\,10^{-2}$	$8.39\,10^{-3}$	$6.88\,10^{-3}$	$9.41\,10^{-3}$
B_2	–	–0.543	–0.3427	–0.53	–0.525	–0.294
C_1	–	16.17	11.66	15.49	16.1599	16.08
C_2	°C	10.65	39.17	20.12	21.3989	43.00

A.3 High-Shear Viscosity

As the ultrasonic viscometer is a high-shear viscometer, it was important to take into account any shear-thinning behaviour from the fluids. For all shear-thinning models, the Cox-Merz law was applied and the resonance frequency (4.5 MHz) was used as the shear rate ($4.5 \times 10^6\ s^{-1}$). The cyclic frequency f was used rather than the angular frequency ω, as recommended by Bair et al. (2018).

Water and **octane** (C_8H_{18}) are both made of small molecules, they were thus considered to have a Newtonian behaviour: their low-shear viscosity was used. No model was found in the literature for the shear-thinning behaviour of **DidP**: the low-shear viscosity was used.

SQL has a shear-thinning behaviour at high shear rate. Bair et al. (2014) proposed a steady-shear Carreau model, which was applied to the WLF-Yasutomi model. At 40 °C, the low-shear and high-shear viscosities are identical up to 200 MPa. The high-shear viscosity is then lower than the low-shear one. In Eq. 8, η is the high-shear viscosity, μ is the low-shear viscosity from the WLF-Yasutomi model, $\dot{\gamma}$ is the shear rate, and $G = 7$ MPa and $n = 0.46$ for the steady shear of SQL. As done by Bair (2006), the single-plateau Carreau equation was used as the second plateau was not observed.

$$\eta(\dot{\gamma}) = \mu \left[1 + \left(\frac{\mu\dot{\gamma}}{G}\right)^2\right]^{\frac{n-1}{2}} \tag{8}$$

SQL+PIP is a shear thinning fluid. Similarly to SQL, the Carreau model proposed by Bair (2006) was applied to the WLF-Yasutomi model (8). This time, G is defined using (9), with $n = 0.8$, $G_R = 10$ kPa, $\mu_R = 0.0711$ Pas, and $m = 0$ for the steady-shear viscosity of SQL+PIP.

$$G = G_R \left(\frac{\mu}{\mu_R}\right)^m \tag{9}$$

The shear-thinning model from Bair and Flores-Torres (2019) was used to compute the steady-shear viscosity of **PAO100**. In Eq. 10, the steady-shear viscosity η is expressed as a function of the low-shear viscosity μ from the WLF-Yasutomi model, the shear stress σ, and the parameters

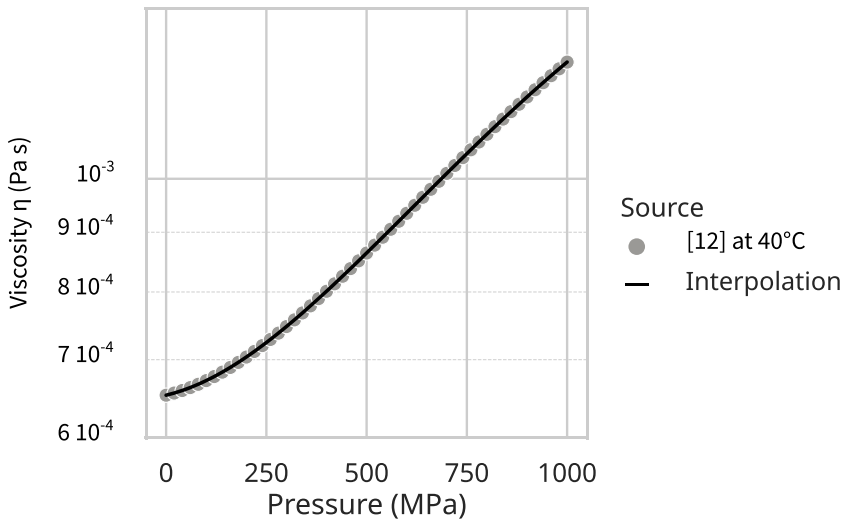

Fig. 12 Viscosity-pressure behaviour of distilled water at 40 °C

for PAO100: $G_1 = 22\,\text{kPa}$, $G_2 = 5080\,\text{kPa}$, $n_1 = 0.89$, $n_2 = 0.52$. The shear stress σ was selected so that the shear rate $\dot{\gamma}$ was equal to $4.5 \times 10^6\,\text{s}^{-1}$ using $\dot{\gamma} = \frac{\sigma}{\eta}$.

$$\eta(\sigma) = \mu \left[1 + \left(\frac{\sigma}{G_1}\right)^2\right]^{\frac{n_1-1}{2n_1}} \left[1 + \left(\frac{\sigma}{G_2}\right)^2\right]^{\frac{n_2-1}{2n_2}} \tag{10}$$

Acknowledgements The authors thank Bianca Aigner for her support in conducting the experimental procedure.
This work was carried out as part of the COMET Centre InTribology project (FFG no. 906860). InTribology is funded within the COMET – Competence Centres for Excellent Technologies Programme by the federal ministries BMIMI and BMWET as well as the federal states of Niederösterreich and Vorarlberg based on financial support from the project partners involved. COMET is managed by FFG.

References

Bair S (2000) Pressure-viscosity behavior of lubricants to 1.4 GPa and its relation to EHD traction. Tribol Trans 43:91–99. https://doi.org/10.1080/10402000008982317

Bair S (2002) The high pressure rheology of some simple model hydrocarbons. Proc Inst Mech Eng J J Eng Tribol 216(3):139–149. https://doi.org/10.1243/1350650021543960

Bair S (2006) Reference liquids for quantitative elastohydrodynamics: selection and rheological characterization. Tribol Lett 22(3):197–206. https://doi.org/10.1007/s11249-006-9083-y

Bair S, Flores-Torres S (2019) The viscosity of polyalphaolefins mixtures at high pressure and stress. J Tribol 141(2). ISSN: 15288897. https://doi.org/10.1115/1.4041124

Bair S et al (2013) An improved yasutomi correlation for viscosity at high pressure. Proc Inst Mech Eng J J Eng Tribol 227(9):1056–1060. https://doi.org/10.1177/1350650112474394

Bair S, Yamaguchi T, Brouwer L et al (2014) Oscillatory and steady shear viscosity: the cox-merz rule, superposition, and application to ehl friction. Tribol Int 79:126–131. https://doi.org/10.1016/J.TRIBOINT.2014.06.001

Bair S et al (2018) New ehl modeling data for the reference liquids squalane and squalane plus polyisoprene. Tribol Trans 61(2):247–255. https://doi.org/10.1080/10402004.2017.1310339

Caetano FJ et al (2004) Viscosity of di-isodecylphthalate: a potential standard of moderate viscosity. Int J Thermophys 25(5):1311–1322. https://doi.org/10.1007/s10765-004-5740-2

Caetano FJ et al (2005) New measurements of the viscosity of diisodecyl phthalate using a vibrating wire technique. J Chem Eng Data 50(6):1875–1878. https://doi.org/10.1021/je050151n

Caudwell DR et al (2009) Viscosity and density of five hydrocarbon liquids at pressures up to 200 MPa and temperatures up to 473 K. J Chem Eng Data 54(2):359–366. https://doi.org/10.1021/je800417q

Ciotta F et al (2009) Viscosity and density of carbon dioxide + 2, 6, 10, 15, 19, 23-hexamethyltetracosane (squalane). J Chem Eng Data 54(9):2436–2443. https://doi.org/10.1021/je800894y

Comuñas M et al (2013) Reference correlation of the viscosity of squalane from 273 to 373 k at 0.1 mpa. J Phys Chem Ref Data 4(3). ISSN: 00472689. https://doi.org/10.1063/1.4812573

Comuñas M et al (2014) Viscosity measurements for squalane at high pressures to 350 mpa from t = (293.15 to 363.15) k. J Chem Thermodyn 69:201–208. https://doi.org/10.1016/J.JCT.2013.10.001

Cox WP, Merz EH (1958) Correlation of dynamic and steady flow viscosities. J Polym Sci 28(118):619–622. https://doi.org/10.1002/POL.1958.1202811812

Doolittle AK, Peterson RH (1951) Preparation and physical properties of a series of n-alkanes. J Am Chem Soc 73(5):2145–2151. https://doi.org/10.1021/ja01149a069

Dymond JH, Young KJ (1981) Transport properties of nonelectrolyte liquid mixtures-V. Viscosity coefficients for binary mixtures of benzene plus alkanes at saturation pressure from 283 to 393 K. Int J Thermophys 2(3). https://doi.org/10.1007/BF00504187

Fröba AP, Leipertz A (2007) Viscosity of diisodecyl phthalate by surface light scattering (sls). J Chem Eng Data 52(5):1803–1810. https://doi.org/10.1021/je7001623

Giller EB, Drickamer HG (1949) Viscosity of normal paraffins near the freezing point. Ind Eng Chem 41(9):2067–2069. https://doi.org/10.1021/ie50477a056

Harris KR (2009) Temperature and pressure dependence of the viscosities of 2-ethylhexyl benzoate, bis(2-ethylhexyl) phthalate, 2,6,10,15,19,23-hexamethyltetracosane (squalane), and diisodecyl phthalate. J. Chem. Eng. Data 54(9):2729–2738. https://doi.org/10.1021/je900284z

Harris KR, Bair S (2007) Temperature and pressure dependence of the viscosity of diisodecyl phthalate at temperatures between (0 and 100) °C and at pressures to 1 gpa. J Chem Eng Data. https://doi.org/10.1021/JE060382

Harris KR, Malhotra R, Woolf LA (1997) Temperature and density dependence of the viscosity of octane and toluene. J Chem Eng Data 42(6):1254–126. https://doi.org/10.1021/je970105q

Huber ML et al (2009) New international formulation for the viscosity of H2O. J Phys Chem Ref Data 38(2):101–125. https://doi.org/10.1063/1.3088050

Irving JB, Barlow AJ (1971) An automatic high pressure viscometer. J Phys E Sci Instrum 4(3):232. https://doi.org/10.1088/0022-3735/4/3/017

Krahn UG, Luft G (1994) Viscosity of several liquid hydrocarbons in the temperature range 298–453 k at pressures up to 200 mpa. J Chem Eng Data 39(4):670–672. https://doi.org/10.1021/je00016a006

Liu Y et al (2008) The shear-thinning elastohydrodynamic film thickness of a two-component mixture. J Tribol 130(2):1–7. https://doi.org/10.1115/1.2842298

Madge EW (1930) The variation of the viscosity of liquid with temperature. J Phys Chem 34(7):1599–1602. https://doi.org/10.1021/j150313a019

Motari MMA et al (2007) Density and viscosity of diisodecyl phthalate c6h4(cooc10h21)2, with nominal viscosity at t = 298 k and p = 0.1 mpa of 87 mpa.s, at temperatures from (298.15 to 423.15) k and pressures up to 70 mpa. J Chem Eng Data 52(4):1233–1239. https://doi.org/10.1021/je600562n

Nakamura Y et al (2016) High-pressure viscosity measurements of polyalphaorefins at elevated temperature. Tribol Online 11(2):444–449. https://doi.org/10.2474/trol.11.444

Oliveira CMBP, Wakeham WA (1992) The viscosity of five liquid hydrocarbons at pressures up to 250 MPa. Int J Thermophys 13(5). https://doi.org/10.1007/BF00503906

Paredes X et al (2009) Study of the effects of pressure on the viscosity and density of diisodecyl phthalate. J Chem Thermodyn 41:1007–1015. https://doi.org/10.1016/j.jct.2009.04.002

Pensado AS et al (2006) High-pressure characterization of dynamic viscosity and derived properties for squalane and two pentaerythritol ester lubricants: pentaerythritol tetra-2-ethylhexanoate and pentaerythritol tetranonanoate. Ind Eng Chem Res 45(7):2394–2404. https://doi.org/10.1021/ie051275w

Peretti G et al (2023) In-situ ultrasonic viscometry of lubricants under temperature and shear. Tribol Int 109210. ISSN: 0301-679X. https://doi.org/10.1016/J.TRIBOINT.2023.109210

Schirru M et al (2015) Viscosity measurement in a lubricant film using an ultrasonically resonating matching layer. Tribol Lett 60(3):1–11. https://doi.org/10.1007/s11249-015-0619-x

Schmidt KA et al (2015) New experimental data and reference models for the viscosity and density of squalane. J Chem Eng Data 60(1):137–150. https://doi.org/10.1021/je5008789

The Engineering Toolbox (2003a) Metals - specific heats. https://www.engineeringtoolbox.com/specific-heat-metals-d_152.html. Accessed: 11 Jul 2025

The Engineering Toolbox (2003b) Specific heat of common liquids and fluids. https://www.engineeringtoolbox.com/specific-heat-fluids-d_151.html. Accessed 11 Jul 2025

Thorpe TE, Rodger JW (1894) X. bakerian lecture: On the relations between the viscosity (internal friction) of liquids and their chemical nature. Philos Trans R Soc Lond A 185:397–710. https://doi.org/10.1098/RSTA.1894.0010

Vergne P (2008) Quelles caractérisations pour quels lubrifiants?

Watts RF, Willette GL (1982) Newtonian multigrade gear lubricants: formulation and performance testing. SAE Tech Pap. ISSN: 26883627. https://doi.org/10.4271/821180

Yasutomi S, Bair S, Winer WO (1984) An application of a free volume model to lubricant rheology I–dependence of viscosity on temperature and pressure. J Tribol 106(2):291–302. https://doi.org/10.1115/1.3260907